Journal of Classical Analysis
Volume 2, Number 2 (2013), 183–203
doi:10.7153/jca-02-15

ASYMPTOTICS OF THE GAUSS HYPERGEOMETRIC FUNCTION WITH LARGE PARAMETERS, I

R. B. PARIS

Abstract. We obtain asymptotic expansions for the Gauss hypergeometric function

$$F(a+\varepsilon_1\lambda, b+\varepsilon_2\lambda; c+\varepsilon_3\lambda; z)$$

as $|\lambda|\to\infty$ when the ε_j are finite by an application of the method of steepest descents, thereby extending previous results corresponding to $\varepsilon_j = 0, \pm 1$. By means of connection formulas satisfied by F it is possible to arrange the above hypergeometric function into three basic groups. In Part I we consider the cases (i) $\varepsilon_1 > 0$, $\varepsilon_2 = 0$, $\varepsilon_3 = 1$ and (ii) $\varepsilon_1 > 0$, $\varepsilon_2 = -1$, $\varepsilon_3 = 0$; the third case ε_1, $\varepsilon_2 > 0$, $\varepsilon_3 = 1$ is deferred to Part II. The resulting expansions are of Poincaré type and hold in restricted domains of the complex z-plane. Numerical results illustrating the accuracy of the different expansions are given.

1. Introduction

The Gauss hypergeometric function is defined by

$$F\left(\begin{matrix}a, b\\ c\end{matrix}; z\right) = \sum_{n=0}^{\infty} \frac{(a)_n (b)_n}{(c)_n n!} z^n, \tag{1.1}$$

where $(a)_n = \Gamma(a+n)/\Gamma(a)$ is the Pochhammer symbol (or rising factorial). The infinite series in (1.1) is defined in $|z| < 1$ when $c \neq 0, -1, -2, \ldots$, unless one of the numeratorial parameters equals a negative integer $-m$, in which case the function reduces to a polynomial in z of degree m.

The asymptotic expansion of the Gauss hypergeometric function for large $|z|$ follows in a straightforward manner from the transformation formula

$$F\left(\begin{matrix}a, b\\ c\end{matrix}; z\right) = \frac{\Gamma(c)\Gamma(b-a)}{\Gamma(b)\Gamma(c-a)}(-z)^{-a} F\left(\begin{matrix}a, a-c+1\\ a-b+1\end{matrix}; \frac{1}{z}\right)$$
$$+\frac{\Gamma(c)\Gamma(a-b)}{\Gamma(a)\Gamma(c-b)}(-z)^{-b} F\left(\begin{matrix}b, b-c+1\\ b-a+1\end{matrix}; \frac{1}{z}\right),$$

where $|\arg(1-z)| < \pi$, together with the series expansion in (1.1). The asymptotic behaviour of the function when one or more of the parameters a, b or c are large, with

Mathematics subject classification (2010): Primary 33C05, 34E05, 41A60.
Keywords and phrases: Hypergeometric functions, asymptotic expansion, large parameters.

Paper JCA-02-15

the variable z bounded, is more complicated. An exception is the case when only the parameter c is large, where [11, p. 397]

$$F\left(\begin{matrix}a,b\\ c+\lambda\end{matrix};z\right)\sim\frac{\Gamma(c+\lambda)}{\Gamma(c-b+\lambda)}\sum_{k=0}^{\infty}\frac{d_k(z)(b)_k}{\lambda^{k+b}} \tag{1.2}$$

as $|\lambda|\to\infty$, where

$$d_0(z)=1,\qquad d_1(z)=az+\tfrac{1}{2}(1+b-2c),$$

with higher coefficients obtained from the generating function in [11, Eq. (15.12.4)]. When $|\arg(1-z)|<\pi$, the expansion holds in the sector $|\arg\lambda|\leqslant\frac{1}{2}\pi-\delta$, $\delta>0$, whereas when z is restricted to the half-plane Re $(z)\leqslant\frac{1}{2}$, the expansion holds in the wider sector $|\arg\lambda|\leqslant\pi-\delta$.

In 1918, Watson [19] obtained the asymptotic expansion of the function

$$F\left(\begin{matrix}a+\varepsilon_1\lambda, b+\varepsilon_2\lambda\\ c+\varepsilon_3\lambda\end{matrix};z\right) \tag{1.3}$$

for $|\lambda|\to\infty$ when ε_j have the values 0, ±1. In the following we shall characterise this function by the set $(\varepsilon_1,\varepsilon_2,\varepsilon_3)$ where, by a rescaling of λ, one of the ε_j can always be replaced by unity. By means of the connection formulas for the various solutions of the hypergeometric differential equation, he reduced the problem to the consideration of the following 4 cases: (i) $(0,0,1)$, (ii) $(1,-1,0)$, (iii) $(0,-1,1)$ together with the additional case (iv) $(1,2,0)$. Watson also considered two other cases in which one of the $\varepsilon_j\neq\pm1$, namely $(1,1,2)$ and $(1,1,3)$. The first of these additional cases was the problem considered by Riemann [16] in a fragmentary (posthumous) paper in which he introduced the saddle-point method in the complex plane; see also [14, pp. 202–205] for details. Watson employed contour integral representations of the hypergeometric function and obtained their asymptotic expansion for large $|\lambda|$ by application of the method of steepest descents. The resulting Poincaré-type expansions suffer from small z-regions of validity since they break down in the neighbourhood of critical values of z. A summary of these expansions is given in [18].

An approach that remedies this defect, but at the cost of increased complexity in the coefficients, is the use of uniform expansions. In [3], Jones employed the hypergeometric differential equation to deal with the case $(1,-1,0)$ arising in electromagnetic diffraction problems [15, 2]. The resulting uniform expansion involved the modified Bessel functions and this was extended to deal with the case $(1,1,2)$. Olde Daalhuis [7, 8] employed contour integral representations of the hypergeometric function to develop uniform expansions involving parabolic cylinder and Airy functions for the cases $(0,-1,1)$ and $(1,2,0)$. In [9], this approach was extended to deal with other cases with $\varepsilon_j=0,\pm1$, including the case $(1,1,3)$; see also [11, p. 397].

In this paper, we consider the asymptotic expansion of (1.3) as $|\lambda|\to\infty$ when the non-zero ε_j are not restricted throughout to the values ±1 and the complex variable z is finite and restricted to lie in $|\arg(1-z)|<\pi$. Use of the connection formulas given in Section 2 shows that it is sufficient to consider only the three cases (i) (ε_1, 0, 1),

(ii) $(\varepsilon_1,-1,0)$ and (iii) $(\varepsilon_1,\varepsilon_2,1)$, where $\varepsilon_1>0$, $\varepsilon_2>0$. An application of the expansion of a hypergeometric function corresponding to $(\varepsilon_1,\varepsilon_1,1)$ with $\varepsilon_1>0$ has arisen in aerodynamics [1, 5]. We employ the method of steepest descents applied to contour integral representations of the hypergeometric function in (1.3). The expansions so obtained are of Poincaré type and, although their z-domains of validity are consequently restricted, considerable valuable information is nevertheless gained by such an approach which lays the foundation for further investigation.

2. The three basic types of hypergeometric function

There are in total 20 sets of values of $(\varepsilon_1,\varepsilon_2,\varepsilon_3)$ when *two or more* of the ε_j are non-zero, but 4 of these sets corresponding to one of the $\varepsilon_j=0$ may be removed on account of the symmetry of the hypergeometric function in its two numeratorial parameters

$$F\left(\begin{matrix}a,b\\c\end{matrix};z\right)=F\left(\begin{matrix}b,a\\c\end{matrix};z\right).$$

The remaining 16 sets of values are listed in Table 1, where they are arranged into three separate groups. By means of the connection formulas labelled (T1)–(T3) below, it will be sufficient to consider the expansion of the function in (1.3) for just one set of values of $(\varepsilon_1,\varepsilon_2,\varepsilon_3)$ from each group.

Table 1: The different cases with two or more large parameters. The second column in each type indicates the transformations required to reduce the particular case to a hypergeometric function corresponding to the first entry. A case marked by an asterisk denotes that it is equivalent to the case immediately above it.

Type A				Type B			
ε	0	1		ε	1	0	
$-\varepsilon$	0	1	T1	$-\varepsilon$	1	0	T1
ε	0	-1	T1, T2	ε	-1	0	T1*
$-\varepsilon$	0	-1	T1, T2	$-\varepsilon$	-1	0	T1
Type C							
ε_1	ε_2	1		ε_1	ε_2	-1	T1, T2
$-\varepsilon_1$	ε_2	1	T1	$-\varepsilon_1$	ε_2	-1	T1, T3
ε_1	$-\varepsilon_2$	1	T1*	ε_1	$-\varepsilon_2$	-1	T1, T3*
$-\varepsilon_1$	$-\varepsilon_2$	1	T1	$-\varepsilon_1$	$-\varepsilon_2$	-1	T1, T3

The required connection formulas are

$$F\left(\begin{matrix}a,b\\c\end{matrix};z\right)=(1-z)^{-b}F\left(\begin{matrix}c-a,b\\c\end{matrix};\frac{z}{z-1}\right)=(1-z)^{c-a-b}F\left(\begin{matrix}c-a,c-b\\c\end{matrix};z\right),\quad\text{(T1)}$$

together with

$$F\left(\begin{matrix}a,b\\c\end{matrix};z\right)=\frac{-\Gamma(c-1)\Gamma(a-c+1)\Gamma(b-c+1)}{\Gamma(a)\Gamma(b)\Gamma(1-c)}z^{1-c}(1-z)^{c-a-b}F\left(\begin{matrix}1-a,1-b\\2-c\end{matrix};z\right)$$
$$+\frac{\Gamma(a-c+1)\Gamma(b-c+1)}{\Gamma(a+b-c+1)\Gamma(1-c)}F\left(\begin{matrix}a,b\\a+b-c+1\end{matrix};1-z\right) \tag{T2}$$

and

$$F\left(\begin{matrix}a,b\\c\end{matrix};z\right)=e^{\pi ic}\frac{\Gamma(c-1)\Gamma(b-c+1)\Gamma(1-a)}{\Gamma(b)\Gamma(c-a)\Gamma(1-c)}z^{1-c}(1-z)^{c-a-b}F\left(\begin{matrix}1-a,1-b\\2-c\end{matrix};z\right)$$
$$+e^{\pi i(c-a)}\frac{\Gamma(1-a)\Gamma(b-c+1)}{\Gamma(1-c)\Gamma(b-a+1)}z^{a-c}(1-z)^{c-a-b}F\left(\begin{matrix}1-a,c-a\\b-a+1\end{matrix};\frac{1}{z}\right). \tag{T3}$$

Table 1 shows the connection formulas necessary for expressing the hypergeometric function in (1.3) corresponding to a particular set $(\varepsilon_1,\varepsilon_2,\varepsilon_3)$ in terms of the first-listed set in each group. We begin by considering Type A in Section 3. However, for convenience in presentation in Section 4 when discussing the functions belonging to Type B, we shall find it more convenient to adopt the set of values $(\varepsilon,-1,0)$ as the standard case. Functions belonging to Type C are considered in the sequel to this paper [13].

For future reference, we collect together the integral representations of the Gauss hypergeometric function $F(a,b;c;z)$ that we shall require in our investigation; see, for example, [17, pp. 20–22], [11, p. 388]. These are

$$F\left(\begin{matrix}a,b\\c\end{matrix};z\right)=\frac{\Gamma(c)}{\Gamma(a)\Gamma(c-a)}\int_0^1\frac{t^{a-1}(1-t)^{c-a-1}}{(1-zt)^b}dt,\quad \mathrm{Re}(c)>\mathrm{Re}(a)>0, \tag{2.1}$$

$$=\frac{\Gamma(c)\Gamma(1+a-c)}{2\pi i\Gamma(a)}\int_0^{(1+)}\frac{t^{a-1}(t-1)^{c-a-1}}{(1-zt)^b}dt,\quad \mathrm{Re}(a)>0, \tag{2.2}$$

where it supposed in each case that $|\arg(1-z)|<\pi$ and that in (2.2) $c-a\neq 1,2,\ldots$ and, in addition, that the integration path does not enclose the point $t=1/z$.

3. The expansion for hypergeometric functions of Type A

We first consider the hypergeometric function in (1.3) corresponding to the set of values $(\varepsilon,0,1)$ with $\varepsilon>0$. The case $\varepsilon=1$ may be excluded since, by means of the first of the transformations (T1), this reduces to a case of (1.2). We consider separately the situations corresponding to $0<\varepsilon<1$ and $\varepsilon>1$; the expansions so developed will not be valid, however, in the limits $\varepsilon\to 0$ and $\varepsilon\to 1$.

3.1. The case $0<\varepsilon<1$

From (2.1), we take as our starting point the integral representation

$$F_1(\lambda;z)\equiv F\left(\begin{matrix}a+\varepsilon\lambda,b\\c+\lambda\end{matrix};z\right)=\frac{\Gamma(c+\lambda)}{\Gamma(a+\varepsilon\lambda)\Gamma(c-a+(1-\varepsilon)\lambda)}\int_0^1 f(t)\,e^{\lambda\psi(t)}dt, \tag{3.1}$$

where the phase factor $\psi(t)$ and amplitude function $f(t)$ are

$$\psi(t) = \varepsilon \log t + (1-\varepsilon)\log(1-t), \qquad f(t) = \frac{t^{a-1}(1-t)^{c-a-1}}{(1-zt)^b} \tag{3.2}$$

and $|\arg(1-z)| < \pi$. The parameter λ is a large complex variable which, for the moment, we shall suppose satisfies $|\arg\lambda| < \frac{1}{2}\pi$. The condition in (2.1) on the parameters is satisfied as $|\lambda| \to \infty$ in $|\arg\lambda| < \frac{1}{2}\pi$. The t-plane is cut along $(-\infty, 0]$ and $[1, +\infty)$ and from $t = 1/z$ to infinity in a suitable direction.

The phase factor in (3.2) has saddle points where $\psi'(t) = 0$; that is, at the point $t_s = \varepsilon$. For sufficiently large $|\lambda|$ in $|\arg\lambda| < \frac{1}{2}\pi$, the points $t = 0$ and $t = 1$ are zeros of the integrand, so that paths of steepest descent can terminate only at these two points; paths of steepest ascent must terminate at infinity. A typical arrangement of the steepest paths through t_s when $0 < \varepsilon < 1$ is shown in Fig. 1(a), (b). The path of steepest descent through t_s is easily verified to have the directions $\arg t = -\frac{1}{2}\arg\lambda$ and $\arg t = \pi - \frac{1}{2}\arg\lambda$. When $\arg\lambda = 0$, the path of steepest ascent through t_s passes to infinity in the directions $\arg t = \pm(1-\varepsilon)\pi$, but when $\arg\lambda \neq 0$ the approach to infinity, as with the approach of the path of steepest descent towards the endpoints $t = 0$ and $t = 1$, is in a spiral manner, possibly crossing over onto adjacent Riemann sheets.

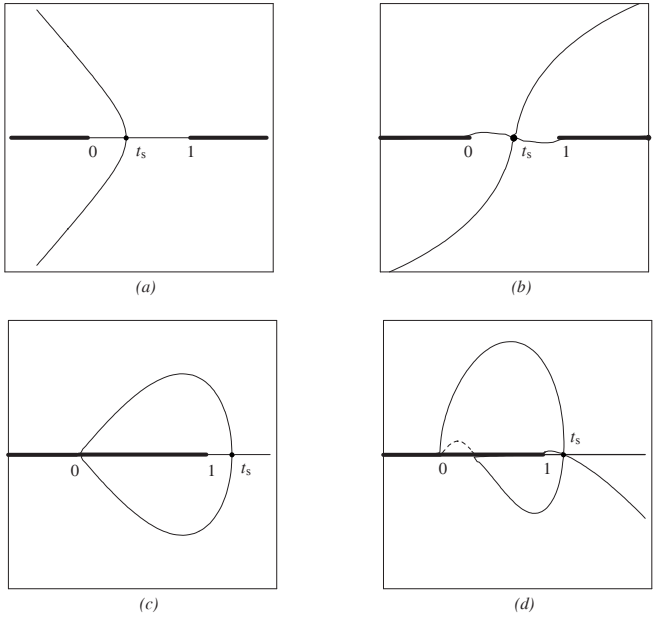

Figure 1: *Paths of steepest descent and ascent through the saddle t_s when (a) $\varepsilon = 0.25$, $\arg\lambda = 0$, (b) $\varepsilon = 0.50$, $\arg\lambda = 0.15\pi$, (c) $\varepsilon = 1.20$, $\arg\lambda = 0$ and (d) $\varepsilon = 1.20$, $\arg\lambda = 0.10\pi$. The heavy lines denote branch cuts and the dot the saddle point. The dashed part of the curve in (d) signifies that the path has passed on to an adjacent sheet.*

The contribution to the integral (3.1) (without the pre-factor) from the saddle point is then

$$f(t_s)e^{\lambda\psi(t_s)}\sqrt{\frac{2\pi}{|\psi''(t_2)|}}\sum_{k=0}^{\infty}\frac{c_k\Gamma(k+\frac{1}{2})}{\lambda^{k+\frac{1}{2}}\Gamma(\frac{1}{2})} \qquad (0<\varepsilon<1) \tag{3.3}$$

as $|\lambda|\to\infty$, where

$$\psi(t_s)=\log\{\varepsilon^{\varepsilon}(1-\varepsilon)^{1-\varepsilon}\}, \qquad \psi''(t_s)=-\frac{1}{\varepsilon(1-\varepsilon)}$$

and the coefficients c_k for $k\leqslant 2$ are given by

$$c_0=1, \qquad c_1=-\frac{1}{\psi''}\left\{\frac{f''}{f}-\frac{\psi'''f'}{\psi''f}+\frac{1}{4}\left(\frac{5\psi'''^2}{3\psi''^2}-\frac{\psi^{iv}}{\psi''}\right)\right\}, \tag{3.4}$$

$$\begin{aligned}c_2=\frac{1}{\psi''^2}\Bigg\{&\frac{f^{iv}}{6f}-\frac{5\psi'''f'''}{9\psi''f}+\frac{5}{12}\left(\frac{7\psi'''^2}{3\psi''^2}-\frac{\psi^{iv}}{\psi''}\right)\frac{f''}{f}-\frac{35}{36}\left(\frac{\psi'''^3}{\psi''^3}-\frac{\psi'''\psi^{iv}}{\psi''^2}+\frac{6\psi^{v}}{35\psi''}\right)\frac{f'}{f}\\&+\frac{35}{36}\left(\frac{11\psi'''^4}{24\psi''^4}-\frac{3}{4}\left(\frac{\psi'''^2}{\psi''^2}-\frac{\psi^{iv}}{6\psi''}\right)\frac{\psi^{iv}}{\psi''}+\frac{\psi'''\psi^{v}}{5\psi''^2}-\frac{\psi^{vi}}{35\psi''}\right)\Bigg\},\end{aligned} \tag{3.5}$$

with ψ, f and their derivatives being evaluated at $t=t_s$; see, for example, [10, p. 127], [4, p. 119], [12, p. 13].

Then from (3.1) and (3.3), we obtain the expansion when $0<\varepsilon<1$

$$F_1(\lambda;z)\sim\frac{\sqrt{2\pi}\Gamma(c+\lambda)}{\Gamma(a+\varepsilon\lambda)\Gamma(c-a+(1-\varepsilon)\lambda)}\,\frac{\varepsilon^{a-\frac{1}{2}+\varepsilon\lambda}(1-\varepsilon)^{c-a-\frac{1}{2}+(1-\varepsilon)\lambda}}{(1-\varepsilon z)^b}\sum_{k=0}^{\infty}\frac{c_k\Gamma(k+\frac{1}{2})}{\lambda^{k+\frac{1}{2}}\Gamma(\frac{1}{2})} \tag{3.6}$$

as $|\lambda|\to\infty$. It is seen that this expansion ceases to be valid in the neighbourhood of the point $z=1/\varepsilon$.

The large-λ behaviour of $F_1(\lambda;z)$ can also be deduced from the confluence principle discussed in Luke [6, pp. 56–57]. From (1.1) and the fact that $(a+\varepsilon\lambda)_n/(c+\lambda)_n\sim\varepsilon^n$ for large $|\lambda|$, we obtain

$$F_1(\lambda;z)\sim\sum_{n=0}^{\infty}\frac{(b)_n(\varepsilon z)^n}{n!}=(1-\varepsilon z)^{-b}$$

valid in $\varepsilon|z|<1$ by analytic continuation. Application of Stirling's formula

$$\Gamma(a+z)\sim\sqrt{2\pi}z^{z+a-\frac{1}{2}}e^{-z} \qquad (|z|\to\infty,\ |\arg z|<\pi)$$

shows that the factor involving gamma functions appearing in (3.6) has the behaviour

$$\frac{\Gamma(c+\lambda)}{\Gamma(a+\varepsilon\lambda)\Gamma(c-a+(1-\varepsilon)\lambda)}\sim\left(\frac{\lambda}{2\pi}\right)^{1/2}\varepsilon^{\frac{1}{2}-a-\varepsilon\lambda}(1-\varepsilon)^{\frac{1}{2}+a-c-(1-\varepsilon)\lambda}$$

as $|\lambda|\to\infty$. Hence the leading large-λ behaviour of $F_1(\lambda;z)$ from (3.6) correctly reduces to $(1-\varepsilon z)^{-b}$.

3.2. Sectors of validity for complex λ

The expansion in (3.6) results from a Laplace integral and so holds for complex values of λ in $|\arg\lambda| \leqslant \frac{1}{2}\pi - \delta$, $\delta > 0$. The sector of validity of this expansion may now be extended by the device described in [10, p. 114]. This shows that for the Laplace integral

$$\int_0^\infty e^{-\lambda\tau} q(\tau)\, d\tau$$

in which $q(\tau)$ is holomorphic in the sector $-\omega_- < \arg\tau < \omega_+$ (where $\omega_\pm > 0$), its asymptotic expansion for large $|\lambda|$ is valid in the wider sector

$$-\tfrac{1}{2}\pi - \omega_- + \delta \leqslant \arg\lambda \leqslant \tfrac{1}{2}\pi + \omega_+ - \delta. \tag{3.7}$$

The two halves of the integral in (3.1) emanating from the saddle t_s taken along the steepest descent path can be expressed in terms of an integral of the form

$$\int_0^\infty e^{-\lambda\tau} f(t)\frac{dt}{d\tau}\, d\tau, \qquad \tau = -\psi(t) + \psi(t_s) \equiv \Psi(t),$$

where

$$\Psi(t) \equiv \varepsilon \log\frac{\varepsilon}{t} + (1-\varepsilon)\log\left(\frac{1-\varepsilon}{1-t}\right) \tag{3.8}$$

which vanishes at $t = \varepsilon$. The singularities of $f(t)dt/d\tau$ at $t = 0$ and $t = 1$ map to infinity in the τ-plane, with those at $t = \varepsilon$ and $t = 1/z$ occurring at $\tau = 2\pi k i\varepsilon$ and $\tau = \Psi(1/z) + 2\pi k i$, $k = 0, \pm1, \pm2, \ldots$, respectively. If we let

$$\Psi(1/z) \equiv \xi + i\eta, \tag{3.9}$$

where ξ and η are real, then with reference to Fig. 2(a) it follows from (3.7) that, if $\xi \leqslant 0$, then $\omega_\pm = \frac{1}{2}\pi$ and the sector of validity can be extended to $|\arg\lambda| \leqslant \pi - \delta$. If, on the other hand, $\xi > 0$, $\eta \neq 0$ the sector of validity is that in (3.7), where

$$\omega_\pm = \arctan\left(\frac{2\pi \mp \eta}{\xi}\right), \quad \omega_\mp = \pm\arctan(\eta/\xi), \tag{3.10}$$

with the upper or lower signs corresponding respectively to $\eta > 0$ and $\eta < 0$, and arctan denotes an acute angle in each case. If $\xi > 0$, $\eta = 0$, the sector of validity cannot be extended and so is $|\arg\lambda| \leqslant \frac{1}{2}\pi - \delta$.

A simple calculation applied to $\Psi(1/z)$ in (3.8) shows that $\xi \leqslant 0$ when

$$\left|\frac{(z-1)^{1-\varepsilon}}{z}\right| \geqslant \varepsilon^\varepsilon (1-\varepsilon)^{1-\varepsilon}. \tag{3.11}$$

This region in the z-plane is illustrated in Fig. 2(b) and is given by the unshaded domain bounded between the two closed curves. In Table 2, we show the values for different ε of the points labelled A, B, C, D and E in Fig. 2(b), where the node B corresponds to $z = 1/\varepsilon$, C to the intersection of the boundary with the imaginary axis and E represents

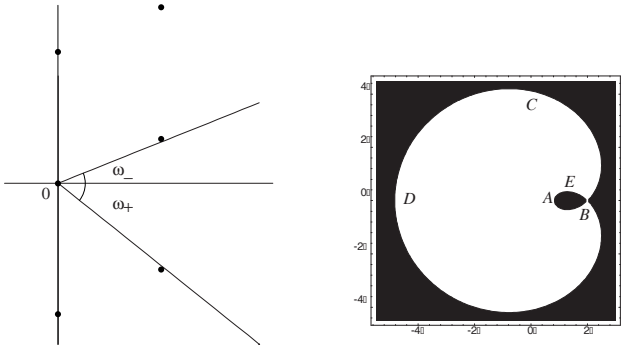

Figure 2: *(a) The singularities (represented by heavy dots) in the τ-plane when $\xi > 0$ and the angles $\omega_{\pm}$. (b) The domain in the z-plane where $\xi \geqslant 0$ (shown shaded) when $0 < \varepsilon < 1$. The particular case shown corresponds to $\varepsilon = 0.50$.*

the maximum value of $\mathrm{Im}(z)$ on the inner loop.[1] If $\xi > 0$, $\eta \neq 0$, that is in the interior of the inner loop and in the exterior of the outer loop, the sector of validity of the expansion (3.2) can be extended to the sector (3.7), with $\omega_{\pm}$ defined in (3.10).

Table 2: Values of $\mathrm{Re}(z)$ at the points labelled A, B and D and $\mathrm{Im}(z)$ at the points labelled C and E in Fig. 2(b) for different values of the parameter ε.

ε	A	B	C	D	E
0.20	0.6736	5.0000	12.3672	15.6411	1.1754
0.25	0.7041	4.0000	9.6351	12.0445	0.9029
0.40	0.7832	2.5000	5.5114	6.6391	0.4838
0.50	0.8284	2.0000	4.1163	4.8284	0.3368
0.60	0.8691	1.6667	3.1687	3.6131	0.2338
0.75	0.9233	1.3333	2.1847	2.3791	0.1237
0.80	0.9399	1.2500	1.9258	2.0633	0.0944

3.3. The case $\varepsilon > 1$

When $\varepsilon > 1$, we employ the integral representation (2.2) to obtain

$$F_1(\lambda;z) = \frac{\Gamma(c+\lambda)\Gamma(1-c+a+(\varepsilon-1)\lambda)}{2\pi i\Gamma(a+\varepsilon\lambda)} \int_0^{(1+)} f(t)e^{\lambda\psi(t)}dt, \tag{3.12}$$

where the integration path is a loop that starts at $t = 0$, encircles the point $t = 1$ in the positive sense (excluding the point $t = 1/z$) and terminates at $t = 0$, and

[1] In the case $\varepsilon = 0.50$, this domain is equivalent to that shown in Fig. 7 of [19, p. 301] with the change of variable $z \to 1 - x$.

$$\psi(t) = \varepsilon \log t + (1-\varepsilon)\log(t-1), \qquad f(t) = \frac{t^{a-1}(t-1)^{c-a-1}}{(1-zt)^b}.$$

The t-plane is cut along $(-\infty, 1]$ and along the ray from $t = 1/z$ to infinity in a suitable direction. The conditions on the parameters in (2.2) are satisfied for $|\lambda| \to \infty$ in $|\arg\lambda| < \frac{1}{2}\pi$. The exponential factor has a saddle point at $t_s = \varepsilon > 1$, where $\psi''(t_s) = \varepsilon^{-1}(\varepsilon-1)^{-1} > 0$. The path of steepest descent through the saddle has the directions $\pm\frac{1}{2}\pi$ at t_s (when $\arg\lambda = 0$) and forms a loop surrounding $t = 1$ with endpoints at $t = 0$. When $\arg\lambda \neq 0$, the loop surrounding $t = 1$ becomes asymmetrical, with part of it crossing the branch cut $[0, 1]$ and passing on to an adjacent Riemann surface; see Fig. 1(c), (d). Then we obtain when $\varepsilon > 1$

$$F_1(\lambda; z) \sim \frac{\Gamma(c+\lambda)\Gamma(1-c+a+(\varepsilon-1)\lambda)}{\Gamma(a+\varepsilon\lambda)} \times \frac{\varepsilon^{a-\frac{1}{2}+\varepsilon\lambda}(\varepsilon-1)^{c-a-\frac{1}{2}+(1-\varepsilon)\lambda}}{\sqrt{2\pi}(1-\varepsilon z)^b} \sum_{k=0}^{\infty} \frac{c_k \Gamma(k+\frac{1}{2})}{\lambda^{k+\frac{1}{2}}\Gamma(\frac{1}{2})} \tag{3.13}$$

as $|\lambda| \to \infty$. Application of Stirling's formula to the ratio of gamma functions shows that the leading large-λ behaviour of $F_1(\lambda; z)$ is again given by $(1-\varepsilon z)^{-b}$.

The domain of validity of the above expansion in the z-plane is largely determined by the requirement that the singularity at $t = 1/z$ should not lie inside the loop of the integration path. It is found that this condition considerably restricts this domain of validity. A straightforward calculation shows that, with $t = \rho e^{i\phi}$, the path of steepest descent through t_s (when $\arg\lambda = 0$) is given by $\operatorname{Im}\psi(t) = 0$ to yield

$$\rho = \frac{\sin\varepsilon\beta}{\sin\beta}, \qquad \beta := \frac{\phi}{\varepsilon-1}.$$

Then the point $1/z$ lies on this path when $z = z_c$, where

$$z_c \equiv z_c(\phi) = \frac{e^{i\phi}\sin\beta}{\sin\varepsilon\beta} \qquad (|\phi| \leqslant (\varepsilon-1)\pi/\varepsilon).$$

In the particular case $\varepsilon = 2$, for example, the steepest descent path through $t = 2$ is described by $\rho = 2\cos\phi$, which is a unit circle centred at $t = 1$, and $\operatorname{Re}(z_c) = \frac{1}{2}$. Then the point $t = 1/z$ lies outside this circle when $\operatorname{Re}(z) < \frac{1}{2}$, therefore restricting the validity of the expansion (3.13) to a half-plane.

Use of the arguments in Section 3.2 shows that the quantity ξ defined in (3.9) satisfies $\xi \leqslant 0$ inside and on the boundary of the loops of the lemniscate

$$|z(1-z)^{\varepsilon-1}| \leqslant \varepsilon^{-\varepsilon}(\varepsilon-1)^{\varepsilon-1};$$

see Fig. 3. The expansion (3.13) breaks down in the neighbourhood of the node $z = 1/\varepsilon$, where the singularity at $t = 1/z$ coincides with the saddle point $t_s = \varepsilon$. Consequently, inside the left-hand loop the expansion (3.13) holds in the sector $|\arg\lambda| \leqslant$

$\pi-\delta$; in the region outside this loop situated on the left of the curve $z=z_c$, the expansion (3.13) holds in the reduced sector (3.7). The determination of the expansion of $F_1(\lambda;z)$ in the neighbourhood of the point $z=1/\varepsilon$ ($\varepsilon>1$) and to the right of the curve $z=z_c$ is not discussed further here.

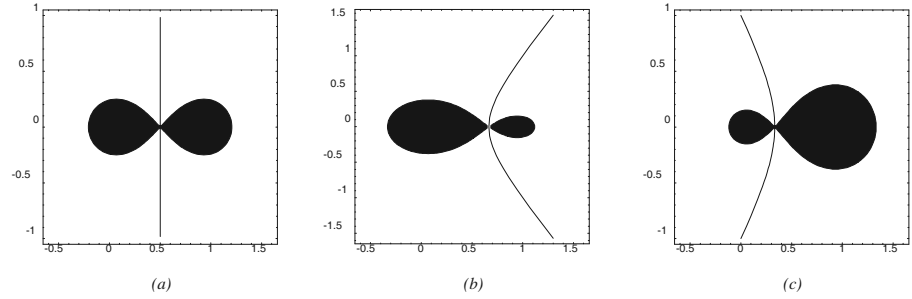

Figure 3: *The domains in the z-plane where $\xi<0$ (shown shaded) when $\varepsilon>1$: (a) $\varepsilon=2$, (b) $\varepsilon=1.50$ and (c) $\varepsilon=3$. The curve passing through the node $z=1/\varepsilon$ corresponds to the points $z=z_c$.*

3.4. Numerical results

In Table 3 we show numerical results[2] for the absolute relative error in $F_1(\lambda;z)$ resulting from the asymptotic expansion (3.6) with the truncation index $k=2$ when z is situated in the domain corresponding to $\xi<0$ in Fig. 2(b). For such values of z the expansion (3.6) holds in the sector $|\arg\lambda|\leqslant\pi-\delta$. In Table 4 we display the errors when z is situated in the domains in Fig. 2(b) where $\xi>0$. In this case, the expansion (3.6) holds in the reduced sector (3.7), where $\omega_\pm$ are computed from (3.10). It can be seen that the relative error starts to deteriorate as the value of $\theta=\arg\lambda$ approaches the boundaries of the sector (3.7).

Finally, in Table 5 we show values of the absolute relative error resulting from the expansion (3.13) with truncation index $k=2$ when $\varepsilon=2$. The first set of values corresponds to a value of z where $\xi<0$, so that the expansion holds in $|\arg\lambda|\leqslant\pi-\delta$, whereas the second set corresponds to $\xi>0$, so that the expansion holds in the reduced sector (3.7).

4. The expansion of hypergeometric functions of Type B

We now consider the hypergeometric function in (1.3) of Type B corresponding to the set of values $(\varepsilon,-1,0)$. From (2.2), we use the integral representation

$$F_2(\lambda;z)\equiv F\left(\begin{matrix}a+\varepsilon\lambda,b-\lambda\\ c\end{matrix};z\right)=\frac{\Gamma(c)\Gamma(1+a-c+\varepsilon\lambda)}{2\pi i\Gamma(a+\varepsilon\lambda)}\int_0^{(1+)}f(t)\,e^{\lambda\psi(t)}dt,\quad(4.1)$$

[2]In the tables we employ the notation $x(-y)$ to denote the number $x\times10^{-y}$.

Table 3: Values of the absolute relative error in $F_1(\lambda;z)$ resulting from the asymptotic expansion (3.6) (with $k \leqslant 2$) for $\lambda = 80e^{i\theta}$ and values of z situated in the domain where $\xi < 0$ in Fig. 2(b), with $a = \frac{1}{3}$, $b = 1$, $c = \frac{3}{4}$.

$z = 0.50 + 0.50i$

θ/π	$\varepsilon = 0.50$	$\varepsilon = 0.75$	θ/π	$\varepsilon = 0.50$	$\varepsilon = 0.75$
0	2.246(−6)	2.736(−6)			
0.20	2.280(−6)	2.750(−6)	−0.20	2.242(−6)	2.771(−6)
0.50	2.366(−6)	2.851(−6)	−0.50	2.292(−6)	2.897(−6)
0.60	2.395(−6)	2.898(−6)	−0.60	2.320(−6)	2.946(−6)
0.80	2.432(−6)	2.989(−6)	−0.80	2.380(−6)	3.024(−6)
0.98	2.286(−6)	3.713(−6)	−0.98	2.530(−6)	3.713(−4)

$z = -1 + i$

θ/π	$\varepsilon = 0.50$	$\varepsilon = 0.75$	θ/π	$\varepsilon = 0.50$	$\varepsilon = 0.75$
0	9.755(−7)	4.383(−7)			
0.20	9.621(−7)	4.298(−7)	−0.20	9.951(−7)	4.460(−7)
0.50	9.613(−7)	4.218(−7)	−0.50	1.021(−6)	4.501(−7)
0.60	9.666(−7)	4.214(−7)	−0.60	1.025(−6)	4.487(−7)
0.80	9.842(−7)	4.248(−7)	−0.80	1.022(−6)	4.419(−7)
0.98	1.206(−6)	3.742(−4)	−0.98	1.276(−6)	3.746(−4)

where the phase factor $\psi(t)$ and amplitude function $f(t)$ are

$$\psi(t) = \varepsilon \log\left(\frac{t}{t-1}\right) + \log(1-zt), \qquad f(t) = \frac{t^{a-1}(t-1)^{c-a-1}}{(1-zt)^b} \tag{4.2}$$

and $|\arg(1-z)| < \pi$. The parameter $\varepsilon > 0$ is finite and λ is a large complex variable which, for the moment, we shall suppose satisfies $|\arg\lambda| < \frac{1}{2}\pi$. The integration path is a loop surrounding the point $t = 1$ in the positive sense which starts and terminates at $t = 0$, but excludes the branch point $t = 1/z$. The t-plane is cut along $[-\infty, 1]$ and along the ray from $1/z$ to infinity in a suitable direction. The conditions in (2.2) on the parameters are satisfied as $|\lambda| \to \infty$ in $|\arg\lambda| < \frac{1}{2}\pi$. We note that when λ is situated in the left half-plane, we may write $\lambda = \varepsilon^{-1}\lambda' e^{\pm\pi i}$, with $|\arg\lambda'| < \frac{1}{2}\pi$, and consider

$$F\left(\begin{matrix} b+\varepsilon^{-1}\lambda', a-\lambda' \\ c \end{matrix}; z\right), \tag{4.3}$$

which is of the same form as the hypergeometric function in (4.1).

Table 4: Values of the absolute relative error in $F_1(\lambda;z)$ resulting from the asymptotic expansion (3.6) (with $k\leqslant 2$) for $\lambda = 80e^{i\theta}$ and values of z situated in the domain where $\xi>0$ in Fig. 2(b), with $a=\frac{1}{2}$, $b=1$, $c=\frac{3}{4}$.

$\varepsilon=0.25\ \ z=1+0.001i$ $\omega_+=0.079\pi,\ \omega_-=0.266\pi$				$\varepsilon=0.75\ \ z=3+5i$ $\omega_+=0.456\pi,\ \omega_-=0.240\pi$			
θ/π	Error	θ/π	Error	θ/π	Error	θ/π	Error
0	1.521(−6)			0	2.574(−6)		
0.20	1.520(−6)	−0.20	1.520(−6)	0.20	2.525(−6)	−0.20	2.600(−6)
0.40	1.517(−6)	−0.40	1.517(−6)	0.50	2.457(−6)	−0.50	2.569(−6)
0.50	1.516(−6)	−0.50	1.515(−6)	0.80	2.434(−6)	−0.60	2.545(−6)
0.55	1.514(−6)	−0.60	1.513(−6)	0.90	2.440(−6)	−0.70	5.867(−4)
0.57	3.536(−2)	−0.70	2.444(−2)	0.93	5.347(−3)	−0.71	8.527(−3)

The phase factor has saddle points where $\psi'(t)=0$; that is, at the points

$$t_{sj}=\Upsilon_\pm=\frac{\varepsilon}{z\Upsilon_\mp}\quad (j=1,2),\qquad \Upsilon_\pm\equiv\Upsilon_\pm(z):=\frac{1+\varepsilon}{2}\left\{1\pm\sqrt{1-\frac{4\varepsilon}{(1+\varepsilon)^2z}}\right\},\tag{4.4}$$

where the upper and lower signs correspond to $j=1$ and $j=2$, respectively. For sufficiently large $|\lambda|$ in $|\arg\lambda|<\frac{1}{2}\pi$, the points $t=0$ and $t=1/z$ are zeros of the integrand, so that paths of steepest descent can terminate only at these points; paths of steepest ascent can therefore terminate only at $t=1$ and at infinity. The contribution to the integral in (4.1) (including the factor $1/(2\pi i)$) from the steepest descent path through the saddle point t_{sj} is given by the formal asymptotic sum

$$f(t_{sj})\frac{e^{\lambda\psi(t_{sj})+\pi i\gamma_j}}{\sqrt{2\pi\psi''(t_{sj})}}\sum_{k=0}^{\infty}\frac{c_k^{(j)}\Gamma(k+\frac{1}{2})}{\lambda^{k+\frac{1}{2}}\Gamma(\frac{1}{2})}\qquad (j=1,2)$$

as $|\lambda|\to\infty$, where

$$\psi''(t_{sj})=\frac{\varepsilon(2t_{sj}-1-\varepsilon)}{t_{sj}^2(t_{sj}-1)^2}$$

and the coefficients $c_k^{(j)}$ for $k\leqslant 2$ are given by (3.4) and (3.5) where ψ, f and their derivatives are evaluated at $t=t_{sj}$ $(j=1,2)$. The γ_j are orientation factors that depend on the direction of integration $\arg(t-t_{sj})$ through the saddle point t_{sj} and have the value either 0 or 1. These factors are determined by

$$\arg(t-t_{sj})=-\tfrac{1}{2}\arg\lambda-\tfrac{1}{2}\arg\psi''(t_{sj})+\begin{cases}\frac{1}{2}\pi\\ -\frac{1}{2}\pi\end{cases},\quad \gamma_j=\begin{cases}0\\1\end{cases},\tag{4.5}$$

where throughout the branch of $\arg\psi''(t_{sj})$ is taken to be $[0,2\pi)$.

Table 5: Values of the absolute relative error in $F_1(\lambda;z)$ when $\varepsilon = 2$ resulting from the asymptotic expansion (3.13) (with $k \leqslant 2$) for $\lambda = 40e^{i\theta}$ with $a = \frac{1}{4}$, $b = \frac{1}{2}$, $c = \frac{3}{4}$.

$z = 0.10 + 0.10i,\ \xi < 0$ $\omega_{\pm} = \frac{1}{2}\pi$				$z = -0.50 + i,\ \xi > 0$ $\omega_{+} = 0.370\pi,\ \omega_{-} = 0.192\pi$			
θ/π	Error	θ/π	Error	θ/π	Error	θ/π	Error
0	4.979(−6)			0	8.093(−6)		
0.20	4.894(−6)	−0.20	5.175(−6)	0.20	4.709(−7)	−0.20	4.811(−7)
0.40	4.931(−6)	−0.40	5.441(−6)	0.40	4.620(−7)	−0.40	4.777(−7)
0.60	5.083(−6)	−0.60	5.680(−6)	0.60	4.551(−7)	−0.60	4.699(−7)
0.80	5.225(−6)	−0.80	5.746(−6)	0.80	4.524(−7)	−0.65	2.439(−6)
0.95	5.527(−6)	−0.95	5.645(−6)	0.86	1.875(−3)	−0.68	2.742(−2)

4.1. Real z

We consider first the case of real z $(= x)$. From (4.4), we see that a double saddle arises when $x = x_*$, where

$$x_* \equiv x_*(\varepsilon) := \frac{4\varepsilon}{(1+\varepsilon)^2}. \tag{4.6}$$

It is evident that $0 < x_*(\varepsilon) \leqslant x_*(1) = 1$ and $x_*(1/\varepsilon) = x_*(\varepsilon)$. Typical paths of steepest descent when $\arg\lambda = 0$ are illustrated in Fig. 4. When $0 < x < x_*$, the saddles are complex with t_{s1} in the upper-half plane and t_{s2} in the conjugate position in the lower-half plane. The steepest descent paths passing over the saddles both emanate from $t = 0$ and terminate at $t = 1/x$, as shown in Fig. 4(a),(e) corresponding to the cases $0 < \varepsilon < 1$ and $\varepsilon > 1$, respectively. The integration path in (4.1) can be deformed to coincide with these steepest descent paths. It then follows that

$$F_2(\lambda;x) \sim \frac{\Gamma(c)\Gamma(1+a-c+\varepsilon\lambda)}{\Gamma(a+\varepsilon\lambda)} \left\{ \frac{f(t_{s1})\, e^{\lambda\psi(t_{s1})+\pi i\gamma_1}}{\sqrt{2\pi\psi''(t_{s1})}} \sum_{k=0}^{\infty} \frac{c_k^{(1)}\Gamma(k+\frac{1}{2})}{\lambda^{k+\frac{1}{2}}\Gamma(\frac{1}{2})} \right.$$
$$\left. + \frac{f(t_{s2})\, e^{\lambda\psi(t_{s2})+\pi i\gamma_2}}{\sqrt{2\pi\psi''(t_{s2})}} \sum_{k=0}^{\infty} \frac{c_k^{(2)}\Gamma(k+\frac{1}{2})}{\lambda^{k+\frac{1}{2}}\Gamma(\frac{1}{2})} \right\} \qquad (0 < x < x_*) \tag{4.7}$$

as $\lambda \to +\infty$, where the orientation factors γ_1 and γ_2 are determined from (4.5) with the loop described in the positive sense.

When $x_* < x < 1$ $(\varepsilon \neq 1)$, the saddles lie on the real axis such that $0 < t_{s2} < t_{s1} < 1$ when $0 < \varepsilon < 1$ and $1/x < t_{s2} < t_{s1}$ when $\varepsilon > 1$, with t_{s2} being the dominant saddle in both cases; see Fig. 4(c),(f). When $0 < \varepsilon < 1$, the steepest descent path between $t = 0$ and $t = t_{s1}$ coincides with the real axis on the lower side of the branch cut, passing over the saddle t_{s2}. At t_{s1}, the steepest path turns through $-\frac{1}{2}\pi$ and terminates at $t = 1/x$.

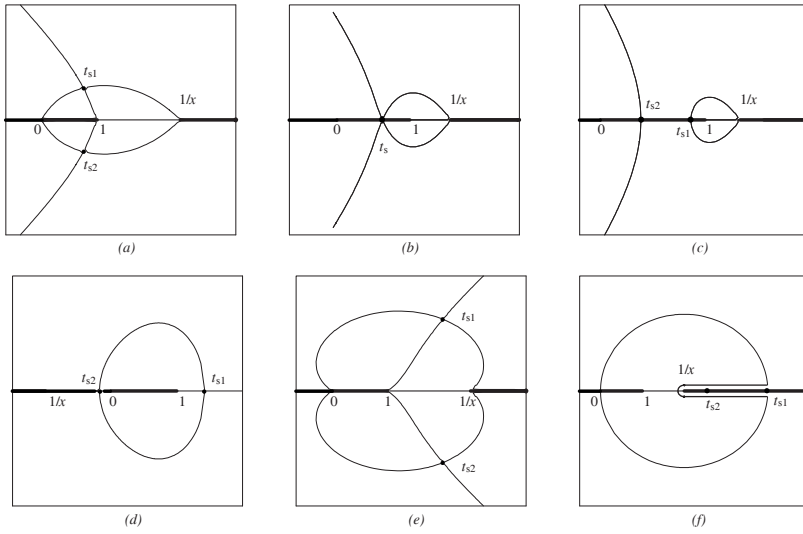

Figure 4: *Paths of steepest descent and ascent when* $\arg\lambda = 0$*: (a)* $0 < x < x_*$*, (b)* $x = x_*$*, (c)* $x_* < x < 1$*, (d)* $x < 0$ *when* $\varepsilon = 0.25$ *(*$x_* = 0.64$*), and (e)* $0 < x < x_*$*, (f)* $x_* < x < 1$ *when* $\varepsilon = 3$ *(*$x_* = 0.75$*). The dots denote the saddle points and the heavy lines are the branch cuts.*

The steepest descent path from $t = 1/x$ in the upper half-plane is the symmetrical image of that in the lower half-plane and passes to the origin over the saddle t_{s2} on the upper side of the branch cut. When $\varepsilon > 1$, the steepest descent path from the origin connects with the saddle t_{s1} on the lower side of the branch cut from $t = 1/x$, and thence passes along the underside of this cut over the saddle t_{s2} to the point $t = 1/x$. The path in the upper half-plane is again the symmetrical image of that in the lower half-plane.

Taking into account the behaviour of the factors $(t_{s2}-1)^{c-a-1-\varepsilon\lambda}$ and $(1-xt_{s2})^{\lambda-b}$ on both sides of the cuts, we obtain the dominant expansion

$$F_2(\lambda;x) \sim 2A\,\frac{\Gamma(c)\Gamma(1+a-c+\varepsilon\lambda)}{\Gamma(a+\varepsilon\lambda)}\,\frac{\hat{f}(t_{s2})\,e^{\lambda\hat{\psi}(t_{s2})}}{\sqrt{2\pi|\psi''(t_{s2})|}}\sum_{k=0}^{\infty}\frac{c_k^{(2)}\Gamma(k+\frac{1}{2})}{\lambda^{k+\frac{1}{2}}\Gamma(\frac{1}{2})} \qquad (4.8)$$

$$(x_* < x < 1),$$

where

$$A = \begin{cases} \sin\pi(\varepsilon\lambda+a-c) & (0<\varepsilon<1) \\ \sin\pi(b-\lambda) & (\varepsilon>1). \end{cases}$$

The quantities $\hat{f}(t)$ and $\hat{\psi}(t)$ are as defined in (4.2), but with the factors $t-1$ and $1-xt$ replaced by $1-t$ $(0<\varepsilon<1)$ and $xt-1$ $(\varepsilon>1)$.

When $\varepsilon\lambda+a-c = \mathbf{N}$, where $\mathbf{N}$ is a positive integer, the sine factor in (4.8) corresponding to the case $0<\varepsilon<1$ vanishes. In this case the contributions taken between the origin and t_{s1} cancel and we are left with the contribution from the subdominant saddle: half the contribution leaving t_{s1} in the lower half-plane and half entering t_{s1} in the upper half-plane. Similarly, when $\lambda-b = \mathbf{N}$ in the case $\varepsilon>1$ the cut from $t = 1/x$

is no longer necessary and the contributions from the lower and upper sides of this cut cancel to leave the subdominant contribution from the saddle t_{s1}. Thus we find in both cases

$$F_2(\lambda;x) \sim \frac{\Gamma(c)\Gamma(1+a-c+\varepsilon\lambda)}{\Gamma(a+\varepsilon\lambda)} \frac{f(t_{s1})\, e^{\lambda\psi(t_{s1})+\pi i\gamma_1}}{\sqrt{2\pi\psi''(t_{s1})}} \sum_{k=0}^{\infty} \frac{c_k^{(1)}\Gamma(k+\frac{1}{2})}{\lambda^{k+\frac{1}{2}}\Gamma(\frac{1}{2})} \tag{4.9}$$

$$(x_* < x < 1;\ \ \varepsilon\lambda + a - c = \mathbf{N}\ (0<\varepsilon<1),\ \lambda - b = \mathbf{N}\ (\varepsilon>1)),$$

where the orientation factor $\gamma_1 = 1\ (0<\varepsilon<1),\ 0\ (\varepsilon>1)$. The expansions (4.7) – (4.9) break down in the neighbourhood of the double saddle point when $x = x_*$; see Fig. 4(b). A uniform expansion is required to cover this situation which it is hoped to investigate in a future paper.

When $x<0$, the saddles are again real with $t_{s1}>1$ and $1/x<t_{s2}<0$ for $\varepsilon>0$; see Fig. 4(d). The steepest descent path through t_{s2} is the negative real axis between the origin and $t = 1/x$ (on both sides of the cut). It follows that, since the saddles are connected, t_{s1} is the dominant saddle. Hence, with $\gamma_1 = 0$, we obtain the dominant expansion

$$F_2(\lambda;x) \sim \frac{\Gamma(c)\Gamma(1+a-c+\varepsilon\lambda)}{\Gamma(a+\varepsilon\lambda)} \frac{f(t_{s1})\, e^{\lambda\psi(t_{s1})}}{\sqrt{2\pi\psi''(t_{s1})}} \sum_{k=0}^{\infty} \frac{c_k^{(1)}\Gamma(k+\frac{1}{2})}{\lambda^{k+\frac{1}{2}}\Gamma(\frac{1}{2})} \qquad (x<0;\ \varepsilon>0). \tag{4.10}$$

4.2. Complex λ and z

When $\arg\lambda \neq 0$, the steepest descent paths in Fig. 4 are modified principally by the introduction of a spiral approach to the singular points $t=0$ and $t=1/x$. In Fig. 5(a), (b) we show typical steepest paths when $\arg\lambda\neq 0$ and $x>0$ (the spiral paths are not indicated). The expansion of $F_2(\lambda;x)$ in this case continues to be given by (4.7) and (4.8).

When z is also complex, the point $t=1/z$ moves off the positive real axis into the complex plane to produce typical steepest paths as illustrated[3] in Fig. 5(c), (d). The expansion of $F_2(\lambda;z)$ is then given by the contribution from both saddles

$$F_2(\lambda;z) \sim \frac{\Gamma(c)\Gamma(1+a-c+\varepsilon\lambda)}{\Gamma(a+\varepsilon\lambda)} \left\{ \frac{f(t_{s1})\, e^{\lambda\psi(t_{s1})+\pi i\gamma_1}}{\sqrt{2\pi\psi''(t_{s1})}} \sum_{k=0}^{\infty} \frac{c_k^{(1)}\Gamma(k+\frac{1}{2})}{\lambda^{k+\frac{1}{2}}\Gamma(\frac{1}{2})} + \frac{f(t_{s2})\, e^{\lambda\psi(t_{s2})+\pi i\gamma_2}}{\sqrt{2\pi\psi''(t_{s2})}} \sum_{k=0}^{\infty} \frac{c_k^{(2)}\Gamma(k+\frac{1}{2})}{\lambda^{k+\frac{1}{2}}\Gamma(\frac{1}{2})} \right\} \tag{4.11}$$

for $|\lambda|\to\infty$, where the orientation factors γ_1 and γ_2 are determined from (4.5). The λ-domain of validity of this expansion is discussed in the next section.

[3]It may be observed that the direction of passage over the subdominant saddle t_{s2} is reversed in Fig. 5(c), (d). This reversal occurs when $\mathrm{Im}\,(\lambda\psi(t_{s1})) = \mathrm{Im}\,(\lambda\psi(t_{s2}))$ which, when $\varepsilon = 0.75$, $z = 0.50 + 0.50i$ is found to correspond to $\arg\lambda \doteq 0.338238\pi$. For this critical value of $\arg\lambda$, the saddles t_{s1} and t_{s2} are connected (a Stokes phenomenon), in a manner similar to that shown in Fig. 4(d), with the steepest ascent path through the *subdominant* saddle t_{s2} bending round to become the steepest descent path through t_{s1}.

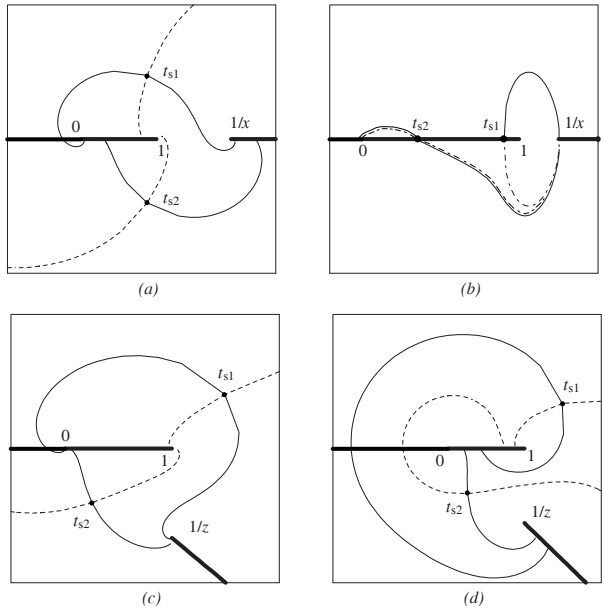

Figure 5: *Typical paths of steepest descent (solid) and ascent (dashed) for complex* λ*: (a)* $\varepsilon = 0.25$ *(*$x_* = 0.64$*),* $x = 0.5$*,* $\arg\lambda = 0.3\pi$*, (b)* $\varepsilon = 0.25$*,* $x = 0.8$*,* $\arg\lambda = 0.1\pi$*, (c)* $\varepsilon = 0.75$*,* $z = 0.5 + 0.5i$*,* $\arg\lambda = 0.2\pi$ *and (d)* $\varepsilon = 0.75$*,* $z = 0.5 + 0.5i$*,* $\arg\lambda = 0.4\pi$*. The dots denote the saddle points and the heavy lines are the branch cuts. In (b) the dot-dash curves represent steepest descent paths that have crossed over onto adjacent Riemann sheets. The approach of the steepest descent paths near* $t = 0$ *and* $t = 1/z$ *is a spiral (not shown).*

4.3. Sectors of validity for complex λ

The sector of validity of the expansions in (4.7), (4.8), (4.10) and (4.11) may be extended from the sector $|\arg\lambda| \leqslant \frac{1}{2}\pi - \delta$ by the device described in Section 2.2. The two halves of the integral in (4.1) emanating from a saddle t_{sj} taken along the steepest descent path can be expressed in terms of an integral of the form

$$\int_0^\infty e^{-\lambda\tau} f(t)\frac{dt}{d\tau}\,d\tau, \qquad \tau = -\psi(t) + \psi(t_{sj}) \equiv \Psi_j(t),$$

where

$$\Psi_j(t) \equiv \varepsilon \log\left(\frac{t_{sj}(t-1)}{t(t_{sj}-1)}\right) + \log\left(\frac{1-zt_{sj}}{1-zt}\right) \qquad (j = 1, 2). \tag{4.12}$$

The singularities of $f(t)\,dt/d\tau$ at $t = 0, 1$ and $1/z$ map to infinity; the singularities resulting from $dt/d\tau$ occur at the saddles t_{sj}. For the saddle t_{s1}, the singularities occur at $\tau = 2\pi ki\varepsilon$ and $\Psi_1(t_{s2}) + 2\pi ki$, where $k = 0, \pm 1, \pm 2, \ldots$. If we let

$$\Psi_1(t_{s2}) = \xi + i\eta, \tag{4.13}$$

where ξ and η are real, it follows from Section 2.2 that if $\xi \leqslant 0$ the sector of validity can be extended to $|\arg\lambda| \leqslant \pi - \delta$. If $\xi > 0$, $\eta \neq 0$ the sector of validity is that in

(3.7), where $\omega_{\pm}$ are obtained from (3.10), whereas if $\xi > 0$, $\eta = 0$ the sector of validity cannot be extended and so is $|\arg\lambda| \leqslant \frac{1}{2}\pi - \delta$. An example of the domain surrounding the point $z = 1$ where $\xi < 0$ is shown in Fig. 6; straightforward calculations using (4.4) show that $\xi = 0$ when

$$\left| \left(\frac{1 - 1/\Upsilon_-}{1 - 1/\Upsilon_+} \right)^{\varepsilon} \frac{1 - \varepsilon/\Upsilon_-}{1 - \varepsilon/\Upsilon_+} \right| = 1.$$

This domain shrinks to zero as $\varepsilon \to 1$, since when $\varepsilon = 1$ the above condition reduces to

$$\left| \frac{1 + \sqrt{1 - z^{-1}}}{1 - \sqrt{1 - z^{-1}}} \right| = 1;$$

with $1 - z^{-1} = \rho e^{i\varphi}$, this yields $\rho^{1/2} \cos\frac{1}{2}\varphi = 0$ whence $\rho = 0$ or $\varphi = \pm\pi$. Consequently, when $\varepsilon = 1$, we conclude that the curve on which $\xi = 0$ consists only of the interval $(0, 1]$ in the z-plane.

If we momentarily write $t_{sj} \equiv t_{sj}(\varepsilon)$, $\xi \equiv \xi(\varepsilon)$, then it easily seen from (4.4) and (4.6) that $t_{sj}(\varepsilon) = \varepsilon/(z\Upsilon_{\mp})$ and $t_{sj}(1/\varepsilon) = \varepsilon^{-1} t_{sj}(\varepsilon)$. Substitution of these indentities in $\Psi_1(t_{s2})$ in (4.12) shows that $\xi(1/\varepsilon) = \varepsilon^{-1}\xi(\varepsilon)$. Consequently, it follows that the domain where $\xi < 0$ is the same when ε is replaced by $1/\varepsilon$.

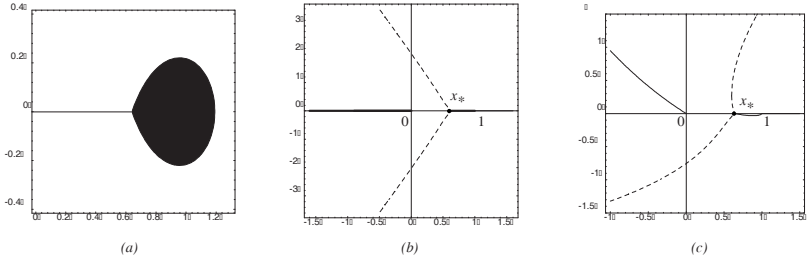

(a) *(b)* *(c)*

Figure 6: *(a) The domain in the z-plane where $\xi < 0$ (shown shaded) when $\varepsilon = 0.25$ and, by the reciprocity relation $\xi(1/\varepsilon) = \varepsilon^{-1}\xi(\varepsilon)$, when $\varepsilon = 4$. Outside this domain $\xi > 0$ except on the line issuing from the node $z = x_*$ where $\xi = 0$. (b) The Stokes curves in the z-plane for $\varepsilon = 0.25$ ($x_* = 0.64$) when $\arg\lambda = 0$ and (c) when $\arg\lambda = 0.1\pi$. The dashed curves indicate inactive Stokes curves for (4.1).*

When the integral (4.1) involves both saddles we conclude that, since $\Psi_1(t_{s2}) = -\Psi_2(t_{s1})$, the sectors of validity of the resulting asymptotic expansion are

$$\arg\lambda \in \begin{cases} (-\frac{1}{2}\pi, \frac{1}{2}\pi) & (\eta = 0,\ \xi \neq 0) \\ (-\pi, \pi) & (\eta \neq 0,\ \xi = 0) \\ (-\frac{1}{2}\pi - \omega_-, \frac{1}{2}\pi + \omega_+) & (\eta \neq 0,\ \xi \neq 0). \end{cases} \tag{4.14}$$

For values of λ in the left-hand half-plane the expansion of $F_2(\lambda; z)$ can be determined from (4.3). We observe that in the case $\eta = 0$ the expansion remains undetermined when $\arg\lambda = \pm\frac{1}{2}\pi$.

4.4. Numerical results

In this section we present the results of numerical calculations of the hypergeometric function $F_2(\lambda;z)$ defined in (4.1) and its various asymptotic representations. For real λ and real values of z $(=x)$ in the three ranges $0<x<x_*$, $x_*<x<1$ and $x<0$, we show the values of $F_2(\lambda;x)$ and the absolute relative error using the truncation index $k=2$ in the asymptotic expansions. The orientation factors γ_j $(j=1,2)$ are indicated. In Table 6 the asymptotic values are obtained from (4.7) when $0<x<x_*$ and from (4.10) when $x<0$. The values shown in Table 7 correspond to the range $x_*<x<1$ and noninteger and integer values of $\varepsilon\lambda+a-c$ (when $\varepsilon<1$) and to noninteger and integer values of $\lambda-b$ (when $\varepsilon>1$). The asymptotic approximations employed are those in (4.8) and (4.9). It is seen that when $\varepsilon\lambda+a-c$ $(\varepsilon<1)$ and $\lambda-b$ $(\varepsilon>1)$ take on integer values, the value of $F_2(\lambda;x)$ decreases several orders of magnitude.

Table 6: Values of $F_2(\lambda;x)$ and the absolute relative error resulting from the asymptotic expansion (4.7) when $0<x<x_*$ and (4.10) when $x<0$ (with $k\leqslant 2$). The values shown correspond to $\lambda=40$ for different a and ε, with $b=\frac{3}{2}$, $c=2$. The values of the orientation factors associated with the expansion (4.7) are $\gamma_1=1$, $\gamma_2=0$.

	$\varepsilon=0.50,\ x=0.25$		$\varepsilon=1,\ x=0.25$		$\varepsilon=3,\ x=0.25$	
a	$F_2(\lambda;x)$	Rel. Error	$F_2(\lambda;x)$	Rel. Error	$F_2(\lambda;x)$	Rel. Error
0.50	1.18363(−4)	8.073(−7)	1.72692(−3)	1.803(−6)	2.16702(2)	2.559(−6)
0.75	−9.29795(−6)	7.270(−5)	8.67525(−4)	3.008(−6)	2.39347(2)	2.489(−6)
1.00	−1.42524(−4)	6.628(−6)	−6.00623(−5)	4.031(−5)	2.62136(2)	2.441(−6)
	$\varepsilon=0.50,\ x=-0.50$		$\varepsilon=1,\ x=-0.50$		$\varepsilon=3,\ x=-0.50$	
a	$F_2(\lambda;x)$	Rel. Error	$F_2(\lambda;x)$	Rel. Error	$F_2(\lambda;x)$	Rel. Error
0.50	1.65375(15)	1.029(−5)	6.69844(19)	3.538(−6)	8.34099(29)	4.899(−7)
1.00	2.29684(15)	4.959(−6)	8.32655(19)	2.087(−6)	9.25050(29)	3.460(−7)
2.00	4.37104(15)	1.058(−6)	1.28017(20)	7.411(−7)	1.13672(30)	1.826(−7)

Table 7: Values of $F_2(\lambda;x)$ and the absolute relative error resulting from the asymptotic expansions (4.8) and (4.9) (with $k\leqslant 2$) when $x_*<x<1$. The values shown correspond to $\lambda=40$ with $b=\frac{3}{2}$, $c=2$ (upper half) and $a=1$, $c=2$ (lower half).

	$\varepsilon=1/3, x=0.85$		$\varepsilon=1/3, x=0.90$	
a	$F_2(\lambda;x)$	Rel. Error	$F_2(\lambda;x)$	Rel. Error
1.00	−3.21788(−12)	2.684(−3)	−7.30399(−13)	2.564(−4)
2/3	1.72126(−15)	1.030(−3)	1.14450(−19)	1.120(−4)
	$\varepsilon=3, x=0.85$		$\varepsilon=3, x=0.90$	
b	$F_2(\lambda;x)$	Rel. Error	$F_2(\lambda;x)$	Rel. Error
0.50	1.30977(34)	1.398(−4)	2.04883(46)	1.554(−5)
1.00	−3.61444(25)	3.268(−5)	−1.57098(27)	3.070(−6)

Table 8: Values of the absolute relative error in $F_2(\lambda;z)$ resulting from the asymptotic expansions (4.11) and (4.8) (with $k \leqslant 2$) for complex λ and real and complex z, with $\lambda = 40e^{i\theta}$, $a = \frac{1}{2}$, $b = 1$, $c = 2$. In the upper half of the table, conjugate values of $F_2(\lambda;z)$ are obtained for $\theta < 0$. The values of the orientation factors γ_j are determined from (4.5).

θ/π	$\varepsilon = 0.50$, $x = 0.50$ $x_* = 0.889$	$\varepsilon = 2$, $x = 0.50$ $x_* = 0.889$	$\varepsilon = 1/3$, $x = 0.90$ $x_* = 0.75$	$\varepsilon = 3$, $x = 0.90$ $x_* = 0.75$
0	3.864(−6)	3.286(−7)	1.832(−5)	1.428(−6)
0.10	3.779(−6)	7.236(−7)	1.759(−5)	7.293(−6)
0.20	3.664(−6)	7.187(−7)	1.695(−5)	7.213(−6)
0.30	3.570(−6)	7.149(−7)	4.065(−3)	7.098(−6)
0.40	3.501(−6)	7.125(−7)	2.014(−3)	8.717(−6)
0.50	3.463(−6)	7.115(−7)	1.765(−1)	7.339(−1)
θ/π	$\varepsilon = 0.50$, $z = 0.50i$	$\varepsilon = 0.50$, $z = 1+i$	$\varepsilon = 2$, $z = 2+i$	$\varepsilon = 3$, $z = -1+i$
0	3.319(−6)	1.450(−6)	1.219(−7)	5.449(−8)
0.20	3.343(−6)	1.407(−6)	1.216(−7)	5.453(−8)
0.40	3.283(−6)	1.354(−6)	1.209(−7)	5.385(−8)
0.50	3.230(−6)	1.332(−6)	1.204(−7)	5.352(−8)
−0.20	3.226(−6)	3.760(−7)	2.308(−7)	5.506(−8)
−0.40	5.830(−7)	3.606(−7)	4.280(−8)	8.256(−8)
−0.50	5.943(−7)	3.627(−7)	4.286(−8)	4.043(−8)

In the upper half of Table 8 we show values of the absolute relative error in the computation of $F_2(\lambda;x)$ using (4.11) and (4.8) when $x > 0$ with $\lambda = 40e^{i\theta}$ and $0 \leqslant \theta \leqslant \frac{1}{2}\pi$. It is seen that when $x < x_*$, where the quantity η defined in (4.13) satisfies $\eta \neq 0$, the expansion (4.11) remains valid in the sector $|\arg\lambda| \leqslant \frac{1}{2}\pi$, whereas when $x_* < x < 1$, where $\eta = 0$, the expansion (4.8) breaks down near $\theta = \frac{1}{2}\pi$ in accordance with (4.14). In this case the expansion of $F_2(\lambda;z)$ remains undetermined when λ is pure imaginary.

Finally, in the lower half of Table 8 we show values of the absolute relative error in the computation of $F_2(\lambda;z)$ using (4.11) when both λ and z are complex. The value of η in each case is found to be non-zero, so that by (4.14) the expansion is valid in (at least) the sector $|\arg\lambda| \leqslant \frac{1}{2}\pi$. The expansion when λ lies in the left-hand plane can be obtained via (4.3). In Fig. 6(b), (c) we show the Stokes curves in the z-plane for the particular case $\varepsilon = 0.25$ and two values of $\arg\lambda$. These curves correspond to the curves on which $\eta = 0$ and from (4.4) and (4.13) are given by the z values satisfying

$$\operatorname{Im}\left[\varepsilon\log\left(\frac{1-1/\Upsilon_-}{1-1/\Upsilon_+}\right)+\log\left(\frac{1-\varepsilon/\Upsilon_-}{1-\varepsilon/\Upsilon_+}\right)\right]=0.$$

Three curves emanate[4] from the double saddle at $x_* = 0.64$, with one curve being the interval $[x_*, 1]$, and a fourth emanates from the origin and coincides with the negative

[4]Considerable care has to be taken when computing these curves since, when z varies, the argument of

real axis when $\arg\lambda = 0$; these curves become deformed when $\arg\lambda \neq 0$. Two of the Stokes curves emanating from x_* are shown dashed since it is found that on these curves the topology of the steepest descent paths remains unchanged and no Stokes phenomenon occurs for the integral in (4.1). On the solid curves a Stokes phenomenon occurs similar to that depicted in Fig. 4(d): as one crosses these curves the direction of passage over the subdominant saddle t_{s2} is reversed, as typified by Fig. 5(c), (d). Both saddles t_{s1} and t_{s2} contribute to the expansion of $F_2(\lambda;z)$ in (4.11), with t_{s1} being the dominant saddle except for z situated on and in the neighbourhood of the interval $(0,1)$ when $\arg\lambda = 0$. When $\arg\lambda > 0$, the dominant saddle in the upper-half z-plane is t_{s1} whereas t_{s2} is dominant in regions of the lower-half plane; when $\arg\lambda < 0$, this pattern of dominance is reversed.

Acknowledgement.
The author wishes to acknowledge the helpful comments made by the referees.

REFERENCES

[1] T. M. CHERRY, *Asymptotic expansions for the hypergeometric functions occurring in gas-flow theory*, Proc. Roy. Soc. London **A202** (1950) 507–522.
[2] D. S. JONES, *Rawlin's method and the diaphonous cone*, J. Mech. Appl. Math. **53** (2000) 91–109.
[3] D. S. JONES, *Asymptotics of the hypergeometric function*, Math. Meth. Appl. Sci. **24** (2001) 369–389.
[4] R. B. DINGLE, *Asymptotic Expansions: Their Derivation and Interpretation*, Academic Press, London, 1973.
[5] M. J. LIGHTHILL, *The hodograph transformation in trans-sonic flow. II Auxiliary theorems on the hypergeometric functions* $\psi_n(\tau)$, Proc. Roy. Soc. London **A191** (1947) 341–351.
[6] Y. L. LUKE, *The Special Functions and Their Approximation*, Vol. I, Academic Press, New York, 1969.
[7] A. B. OLDE DAALHUIS, *Uniform asymptotic expansions for hypergeometric functions with large parameters, I*, Anal. Appl. (Singap.) **1** (2003) 111–120.
[8] A. B. OLDE DAALHUIS, *Uniform asymptotic expansions for hypergeometric functions with large parameters, II*, Anal. Appl. (Singap.) **1** (2003) 121–128.
[9] A. B. OLDE DAALHUIS, *Uniform asymptotic expansions for hypergeometric functions with large parameters, III*, Anal. Appl. (Singap.) **8** (2010) 199–210.
[10] F. W. J. OLVER, *Asymptotics and Special Functions*, Academic Press, New York, 1974. Reprinted A. K. Peters, Massachussets, 1997.
[11] F. W. J. OLVER, D. W. LOZIER, R. F. BOISVERT AND C. W. CLARK (eds.), *NIST Handbook of Mathematical Functions*, Cambridge University Press, Cambridge, 2010.
[12] R. B. PARIS, *Hadamard Expansions and Hyperasymptotic Evaluation: An Extension of the Method of Steepest Descents*, Encyclopedia of Mathematics and its Applications, Vol. 141, Cambridge University Press, Cambridge, 2011.
[13] R. B. PARIS, *Asymptotics of the Gauss hypergeometric function with large parameters, II*, J. Classical Anal. **3**, 1 (2013), 1–15.
[14] R. B. PARIS AND D. KAMINSKI, *Asymptotics and Mellin-Barnes Integrals*, Cambridge University Press, Cambridge, 2001.
[15] A. D. RAWLINS, *Diffraction by, or diffusion into, a penetrable wedge*, Proc. Roy. Soc. London **A455** (1999) 2655–2686.
[16] B. RIEMANN, *Sullo svolgimento del quoziente di due serie ipergeometriche in funzione continua infinita*, in *Collected Works of Bernhard Riemann* (ed. H. Weber) 145–153, Dover, New York, 1953.

the first logarithm is found to pass on to adjacent Riemann sheets of the log function.

[17] L. J. SLATER, *Generalized Hypergeometric Functions*, Cambridge University Press, Cambridge, 1960.
[18] N. M. TEMME, *Large parameter cases of the Gauss hypergeometric function*, J. Comput. Appl. Math. **153** (2003) 441–462.
[19] G. N. WATSON, *Asymptotic expansions of hypergeometric functions*, Trans. Cambridge Philos. Soc. **22** (1918) 277–308.

(Received March 15, 2013)

R. B. Paris
School of Computing, Engineering and Applied Mathematics
University of Abertay Dundee
Dundee DD1 1HG, UK